Power Reflection and Transmission Coefficients for Meander-Line Polarizers with a Chiral Slab

Kemal Delihacıoğlu and Savaş Uçkun

This paper presents a theoretical investigation of power reflection and transmission coefficients for a meander-line polarizer placed periodically on a chiral slab. It is assumed that a linearly polarized transverse magnetic wave is incident on a chiral slab from the air region. In the analysis, we derive the electric and magnetic fields in the modal form in the air and chiral regions. We obtain power reflection and transmission coefficients in a straightforward manner after matching the tangential components of the electric and magnetic fields at the boundaries. We present numerical results for the power reflection and transmission coefficients versus frequency and incident angle for different values of the chirality admittance. A meander-line polarizer placed on a dielectric slab can convert a linearly polarized wave to a circularly polarized wave. The design parameters for a meander-line polarizer are the dimensions of the meander-line and the values of the dielectric slab. Replacing a dielectric slab with a chiral slab introduces a new independent parameter which controls the wave polarization.

I. INTRODUCTION

Chiral media have received considerable attention in the last decades due to their potential applications in the fields of electromagnetic (EM), microwave, and millimeter wave frequencies. The lack of geometric symmetry between an object and its mirror image is referred to as chirality. An artificial chiral medium for a microwave frequency can be constructed by embedding chiral objects, such as wire helices, möbius strips, and irregular tetrahedrons, in a non-chiral host medium. A linearly polarized wave incident on a chiral slab splits into two circularly polarized waves left and right with different phase velocities. The two circularly polarized waves combine and a linearly polarized wave, whose plane of polarization is rotated with respect to the plane of polarization of the incident plane wave, emerges behind the chiral slab. The amount of rotation or attenuation depends on the distance traveled by the EM wave in the medium and on the difference between the two wave numbers, which is an indication of the degree of chirality given by ξ [1]-[3].

The first meander-line polarizer was designed by trial and error at the Stanford Research Institute in 1966 and the computer program used in its design was described in 1969. Young et al. presented a theoretical analysis and a discussion of the experimental results of a meander-line polarizer [4]. Chu and Lee reported a simple transmission line model in terms of E-and H-type mode for multilayered meander-line polarizers for a plane wave incident at normal and oblique angles [5]. A linearly polarized wave can be converted to a circularly polarized wave with a meander-line polarizer that provides a wide-band circular polarization and a 90° phase difference in transmission between the two linear components. For this purpose, the electric field of the incident wave on a meander-

line polarizer can be seen as consisting of two equal orthogonal components that are respectively parallel ($E_{//}$) and perpendicular ($E_{\perp}$) to the meander-line axis. The $E_{//}$ component is delayed and the $E_{\perp}$ component is advanced due respectively to the inductive and capacitive effects of the grating structure of the meander-line polarizer.

Many researchers have studied the interaction of EM waves with chiral and other possible structures [6]-[11]. However, to the best of our knowledge, no study has dealt with a meander-line polarizer with a chiral slab. The rotation property of chiral media and the polarization property of the meander-line strips motivated us to investigate meander-line polarizers with chiral slabs. Starting out with this curiosity, we made theoretical investigations of the power reflection and transmission coefficients of a meander-line polarizer with a chiral slab for a transverse magnetic (TM) wave incidence.

Assuming it to be infinitely thin and a perfect conductor, we placed a meander-line strip periodically in the x-y plane (Figs. 1(a) and (b)). Due to the periodicity of the problem we expanded the fields into Floquet modes in the air and chiral regions. The boundary conditions, combined with the Floquet modes orthogonality over a single periodic unit cell, lead to a Fredholm integral equation of the first kind for the unknown current density induced on the metallic part of the meander-line by the incident plane wave. This integral equation can be solved using the moments method which entails expanding the unknown current density in terms of a set of basis functions $\{\mathbf{f}_n\}$ and testing with the same basis. We implemented a complex matrix inversion program to obtain the solutions of the resulting matrix equation. We were able to extract the power reflection and transmission coefficients from the electric field equations using the Poynting vector.

II. FORMULATION OF THE PROBLEM

1. Propagation of EM Waves in a Chiral Medium

Assuming an exp(jωt) time dependence, [3] gave the constitutive equations of an isotropic, homogeneous, lossless, and source free chiral medium:

$$\mathbf{D} = \varepsilon_c \mathbf{E} - j\xi \mathbf{B} \tag{1}$$

$$\mathbf{H} = -j\xi \mathbf{E} + \frac{1}{\mu_c} \mathbf{B}, \tag{2}$$

where ε_c, μ_c, and ξ are real constants representing the permittivity, the permeability, and the chirality admittance of the chiral medium, respectively. Using (1) and (2) together with Maxwell's time harmonic equations for a source free region, we obtain the chiral Helmholtz equation as
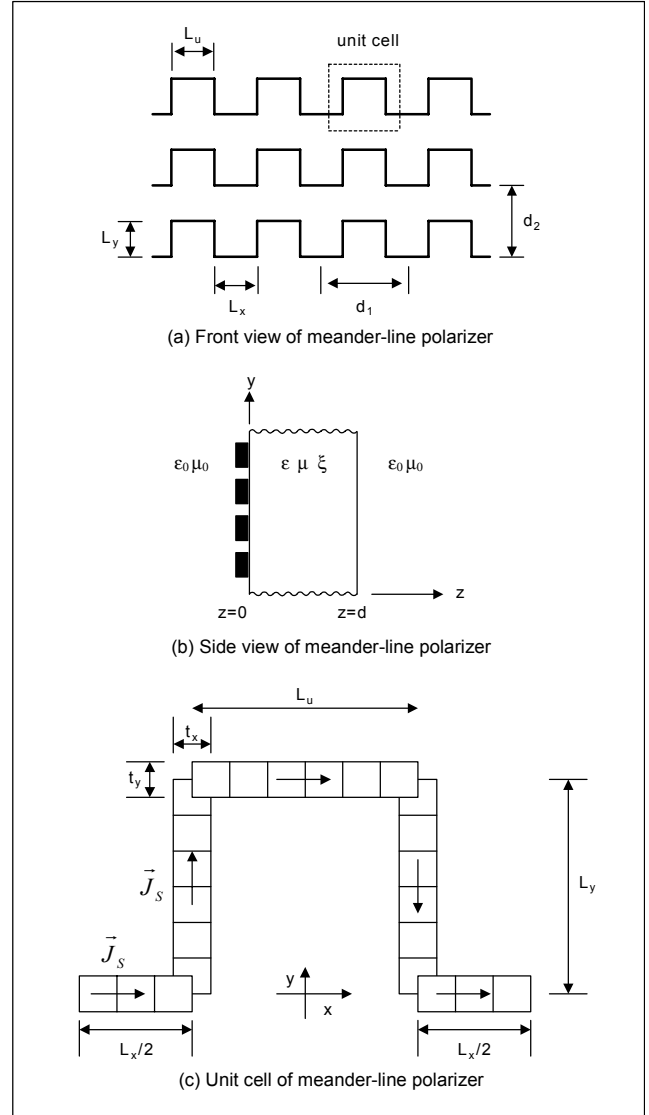

Fig. 1. Geometry of a meander-line polarizer with a chiral slab.

$$\nabla \times \nabla \times \mathbf{E} - 2\omega\mu_c\xi \nabla \times \mathbf{E} - \omega^2\mu_c\varepsilon_c \mathbf{E} = 0 \tag{3}$$

$$\nabla \times \nabla \times \mathbf{H} - 2\omega\mu_c\xi \nabla \times \mathbf{H} - \omega^2\mu_c\varepsilon_c \mathbf{H} = 0. \tag{4}$$

The propagating eigenmodes within such media consist of two circularly polarized waves with characteristic wave numbers,

$$
\begin{aligned}
k_R &= \frac{2\pi}{\lambda_R} = \omega\mu_c\xi + \sqrt{\omega^2\mu_c\varepsilon_c + (\omega\mu_c\xi)^2}, \\
k_L &= \frac{2\pi}{\lambda_L} = -\omega\mu_c\xi + \sqrt{\omega^2\mu_c\varepsilon_c + (\omega\mu_c\xi)^2},
\end{aligned}
\tag{5}
$$

where k_R and k_L are real quantities (wavenumbers) characterizing the right and left circularly polarized waves (RCP

and LCP), respectively. Hence the chiral medium allows a double mode propagation, namely, LCP and RCP waves, which is called polarization birefringence. The LCP and RCP waves propagate with different phase velocities in the chiral medium.

2. Analysis of a Meander-Line Polarizer with a Chiral Slab

The periodic structure of the two-dimensional printed meander-line array is shown in Fig.1(a). The unit cell presented within the dotted line in Fig.1(a) also appears in a larger scale in Fig.1(c). The array is periodic and extends to infinity in both the x and y directions. A unit cell is divided into five branches, three horizontal and two vertical. These branches are also divided into a specific number of segments within a unit cell, as explained by Uckun and Ege [12], and as can be seen in Fig.1(c). It is assumed that a linearly polarized TM wave is incident upon a chiral slab. The total field is the sum of the incident field and the field scattered from the conducting body. The scattered fields are produced by the current distributions on the scatterers. The electromagnetic field distributions near the array of conducting meander-line strips are expanded into a set of Floquet mode functions [13], [14]. Floquet's theorem is an extension of the Fourier series theorem for periodic functions. The extension permits a modal description of any field or function which repeats itself periodically except for a multiplicative exponential factor [13].

Since any rectangular field component $\mathbf{\Psi}$ is well known to be a solution of the homogeneous scalar Helmholtz equation in the given region as

$$\left(\nabla^2 + k^2\right)\mathbf{\Psi}(x, y, z) = 0, \tag{6}$$

where $k^2 = \omega^2 \mu \varepsilon$.

A complete set of solutions of the scalar wave equation can be written for the periodic structure as

$$\mathbf{\Psi} = \sum_{p=-\infty}^{\infty} \sum_{q=-\infty}^{\infty} C_{pq} e^{-j(k_{xo}x + k_{yo}y)} e^{-j(p\mathbf{k}_1 + q\mathbf{k}_2)\cdot\boldsymbol{\rho}} e^{-j\gamma_{pq}z} \tag{7}$$

$$\mathbf{\Psi} = \sum_{p=-\infty}^{\infty} \sum_{q=-\infty}^{\infty} C_{pq} e^{-j\mathbf{k}_{Tpq}\cdot\boldsymbol{\rho}} e^{-j\gamma_{pq}z}, \tag{8}$$

where C_{pq} is a constant and

$$(p\mathbf{k}_1 + q\mathbf{k}_2)\cdot\boldsymbol{\rho} = \frac{2\pi p}{d_1}x + \left(\frac{2\pi q}{d_2} - \frac{2\pi p}{d_1}\right)y$$

$$\mathbf{k}_{Tpq} = \left(k_{xo} + \frac{2\pi}{d_1}p\right)\mathbf{a}_x + \left(k_{yo} - \frac{2\pi}{d_1}p + \frac{2\pi}{d_2}q\right)\mathbf{a}_y \tag{9}$$

$$\gamma_{pq}^2 = k^2 - \mathbf{k}_{Tpq}\cdot\mathbf{k}_{Tpq}, \quad p, q = 0, \pm 1, \pm 2, \pm 3, \ldots,$$

$$k_{xo} = \sin\theta\cos\phi, \quad k_{yo} = \sin\theta\sin\phi,$$

and d_1 and d_2 are the dimensions of the unit cell as shown in Fig.1. The angles θ and ϕ are the standard spherical coordinates.

The total incident fields $(\mathbf{E}_i, \mathbf{H}_i)$ in the first region (z<0) for the incident TM wave can be written as

$$\mathbf{E}_i = E_o^{TM}\mathbf{\Psi}_1 e^{-j\gamma z} + \sum_{m=1}^{2} j^{m-1}E_r^{(m)}\mathbf{\Psi}_m e^{j\gamma z} \tag{10}$$

$$\mathbf{H}_i = \mathbf{a}_z \times \left[Y^{(1)}E_o^{TM}\mathbf{\Psi}_1 e^{-j\gamma z} - \sum_{m=1}^{2} j^{m-1}Y^{(m)}E_r^{(m)}\mathbf{\Psi}_m e^{j\gamma z}\right], \tag{11}$$

where E_o^{TM} is the amplitude of the TM incident wave and $E_r^{(m)}$ is the amplitude of the reflected wave in the absence of a scatterer. The sub- and superscript m=1 and m=2 stand for TM and transverse electric (TE) modes, respectively. The scattered $(\mathbf{E}_s, \mathbf{H}_s)$ fields are

$$\mathbf{E}_s = \sum_{m=1}^{2} \sum_p \sum_q j^{m-1}E_{rpq}^{(m)}e^{j\gamma_{pq}z}\mathbf{\Psi}_{mpq} \tag{12}$$

$$\mathbf{H}_s = -\mathbf{a}_z \times \sum_{m=1}^{2} \sum_p \sum_q j^{m-1}Y_{pq}^m E_{rpq}^{(m)}e^{j\gamma_{pq}z}\mathbf{\Psi}_{mpq}, \tag{13}$$

where $E_{rpq}^{(m)}$ is the amplitude of the scattered field in the first region,

$$Y_{pq}^{(1)} = Y_o\frac{k}{\gamma_{pq}}, \quad \mathbf{\Psi}_{mpq} = \frac{1}{\sqrt{A}}e^{-jk_{Tpq}\cdot\mathbf{r}_T}\mathbf{e}_{mpq}$$

$$\mathbf{e}_{mpq} = \begin{cases} \dfrac{\mathbf{k}_{Tpq}}{|\mathbf{k}_{Tpq}|}, & m=1 \\[3mm] \mathbf{a}_z \times \dfrac{\mathbf{k}_{Tpq}}{|\mathbf{k}_{Tpq}|}, & m=2 \end{cases} \quad Y_{pq}^{(2)} = Y_o\frac{\gamma_{pq}}{k}, \quad Y_o = \sqrt{\frac{\varepsilon_o}{\mu_o}},$$

$A = d_1 d_2$ (periodic cell area) [15].

Inside the chiral slab 0<z<d, the electric and magnetic fields are expressed as the sum of the LCP and RCP plane waves.

$$\mathbf{E}^+ = \sum_{m=1}^{2} \sum_p \sum_q j^{m-1}(A_{Lpq}^{(m)}e^{-j\gamma_{Lpq}z} + (-1)^{m-1}A_{Rpq}^{(m)}e^{-j\gamma_{Rpq}z})\mathbf{\Psi}_{mpq} \tag{14}$$

$$\mathbf{H}^+ = \mathbf{a}_z \times \sum_{m=1}^{2} \sum_p \sum_q j^{m-1}(Y_{Lpq}^{(m)}A_{Lpq}^{(m)}\cdot e^{-j\gamma_{Lpq}z} + (-1)^{m-1}Y_{Rpq}^{(m)}A_{Rpq}^{(m)}\cdot e^{-j\gamma_{Rpq}z})\mathbf{\Psi}_{mpq} \tag{15}$$

$$\mathbf{E}^- = \sum_{m=1}^{2} \sum_p \sum_q (-j)^{m-1}(B_{Lpq}^{(m)}e^{j\gamma_{Lpq}z} + (-1)^{m-1}B_{Rpq}^{(m)}e^{j\gamma_{Rpq}z})\mathbf{\Psi}_{mpq} \tag{16}$$

Kemal Delihacioğlu et al.   **43**

$$\mathbf{H}^- = -\mathbf{a}_z \times \sum_{m=1}^{2} \sum_{p} \sum_{q} (-j)^{m-1} (Y_{Lpq}^{(m)} B_{Lpq}^{(m)} \cdot e^{j\gamma_{Lpq}z}$$
$$+ (-1)^{m-1} Y_{Rpq}^{(m)} B_{Rpq}^{(m)} \cdot e^{j\gamma_{Rpq}z}) \mathbf{\Psi}_{mpq}, \tag{17}$$

where the superscripts + and – represent the +z and –z propagation directions, respectively. The full expressions for the coefficients appearing in (14)-(17) are given in the appendix.

For z>d total transmitted fields $(\mathbf{E}_t, \mathbf{H}_t)$ are given by

$$\mathbf{E}_t = \sum_{m=1}^{2} j^{m-1} (E_t^{(m)} \mathbf{\Psi}_m e^{-j\gamma(z-d)} + \sum_{p} \sum_{q} E_{tpq}^{(m)} e^{-j\gamma_{pq}(z-d)} \mathbf{\Psi}_{mpq}) \tag{18}$$

$$\mathbf{H}_t = \mathbf{a}_z \times \sum_{m=1}^{2} j^{m-1} (Y^{(m)} E_t^{(m)} \mathbf{\Psi}_m e^{-j\gamma(z-d)}$$
$$+ \sum_{p} \sum_{q} Y_{pq}^{(m)} E_{tpq}^{(m)} e^{-j\gamma_{pq}(z-d)} \mathbf{\Psi}_{mpq}), \tag{19}$$

where $E_t^{(m)}$ and $E_{tpq}^{(m)}$ are the amplitudes of the transmitted wave in the absence of the scatterer and the amplitudes of the scattered wave in the third region, respectively. Matching the tangential components of electric and magnetic fields at the boundaries at z=0 and z=d, combined with the orthogonality of the Floquet modes over a unit cell leads to integral equations in which the magnitude of the scattered fields are expressed in terms of the unknown current density:

$$I_{mpq} = \frac{1}{\sqrt{A}} \iint \mathbf{J}_s(x,y) e^{j\mathbf{k}_{Tpq} \cdot \mathbf{r}} \mathbf{e}_{mpq} dx dy, \tag{20}$$

where $\mathbf{r} = x\mathbf{a}_x + y\mathbf{a}_y + z\mathbf{a}_z$ is the position vector. This integral equation can be solved using the moments method which involves expanding the unknown current density in terms of a set of basis functions and testing with the same basis [16]. In order to provide an efficient basis for the induced current we make the approximation that the width of the strips are narrow enough (with respect to λ), so that the component of the current parallel to the width of the strip can be ignored. We assume that the expansion functions are a set of orthogonal pulse functions. In addition, we choose the same functions for the weighting function (Galerkin's method) [17].

$$\mathbf{J}_s = \sum_{n=1}^{N} \alpha_n \mathbf{f}_n(x,y), \tag{21}$$

where α_n are unknown coefficients

$$I_{mpq} = \frac{1}{\sqrt{A}} \iint \sum_{n=1}^{N} \alpha_n \mathbf{f}_n(x,y) \cdot \mathbf{\Psi}_{mpq} dx dy = \sum_{n=1}^{N} \alpha_n \langle \mathbf{f}_n, \mathbf{\Psi}_{mpq} \rangle \tag{22}$$

$$\langle \mathbf{f}_n, \mathbf{\Psi}_{mpq} \rangle = \iint \mathbf{f}_n(x,y) \mathbf{\Psi}_{mpq} dx dy. \tag{23}$$

After finding the current density by evaluating the inner products separately for each branch, the unknown complex coefficients can be found in terms of the current density and the medium parameters. Since both the scattered and incident fields satisfy the air-chiral medium boundary conditions, the only remaining boundary condition is that the total tangential electric field vanishes on the metallic part of the scatterer (meander-line). Therefore at z=0 we have

$$\mathbf{E}_i(x,y,0) + \mathbf{E}_s(x,y,0) = 0 \tag{24}$$

$$\sum_{m=1}^{2} (E_o^{TM} + j^{m-1} E_r^{(m)}) \mathbf{\Psi}_m = -\sum_{m=1}^{2} \sum_{p} \sum_{q} j^{m-1} E_{rpq}^{(m)} \mathbf{\Psi}_{mpq}. \tag{25}$$

Multiplying both sides of the above equation by $\mathbf{f}_1, \mathbf{f}_2, \mathbf{f}_3, ..., \mathbf{f}_n$ successively and then integrating it over a unit cell, we obtain N set of equations:

$$(E_o^{TM} + E_r^{(1)}) < \mathbf{f}_k, \mathbf{\Psi}_1^* > + jE_r^{(2)} < \mathbf{f}_k, \mathbf{\Psi}_2^* >$$
$$= -\frac{1}{A} \sum_{n=1}^{N} \alpha_n \sum_{p} \sum_{q} \{ (r_1 < \mathbf{f}_n, \mathbf{\Psi}_{1pq} >$$
$$+ r_2 < \mathbf{f}_n, \mathbf{\Psi}_{2pq} >) < \mathbf{f}_k, \mathbf{\Psi}_{1pq}^* >$$
$$+ j(r_3 < \mathbf{f}_n, \mathbf{\Psi}_{1pq} > + r_4 < \mathbf{f}_n, \mathbf{\Psi}_{2pq} >) < \mathbf{f}_k, \mathbf{\Psi}_{2pq}^* > \}, \tag{26}$$

where the superscript * stands for the complex conjugate and $k = 1,2,3,...,N$. Eq. (26) is a matrix equation for the unknown coefficients of the current expansion. Upon finding the unknown coefficients α_n by a complex matrix inversion, we can express the total reflected field at z=0 from (10) and (12) as a sum of the reflected fields in the absence of the scatterer and the reflected fields due to the scatterer:

$$\mathbf{E}_r = E_r^{(1)} \mathbf{\Psi}_1 + \frac{1}{\sqrt{A}} \sum_{n=1}^{N} \alpha_n \sum_{p=-\infty}^{\infty} \sum_{q=-\infty}^{\infty} (r_1 < \mathbf{f}_n, \mathbf{\Psi}_{1pq} >$$
$$+ r_2 < \mathbf{f}_n, \mathbf{\Psi}_{2pq} >) \mathbf{\Psi}_{1pq}$$
$$+ j \left[E_r^{(2)} \mathbf{\Psi}_2 + \frac{1}{\sqrt{A}} \sum_{n=1}^{N} \alpha_n \sum_{p=-\infty}^{\infty} \sum_{q=-\infty}^{\infty} (r_3 < \mathbf{f}_n, \mathbf{\Psi}_{1pq} >$$
$$+ r_4 < \mathbf{f}_n, \mathbf{\Psi}_{2pq} >) \mathbf{\Psi}_{2pq} \right]. \tag{27}$$

The transmitted field in the third region can be expressed from (12) and (18) as a sum of the transmitted fields in the absence of the scatterer and the transmitted fields due to the scatterer:

$$\mathbf{E}_t = E_t^{(1)}\mathbf{\Psi}_1 + \frac{1}{\sqrt{A}}\sum_{n=1}^{N}\alpha_n\sum_{p=-\infty}^{\infty}\sum_{q=-\infty}^{\infty}(t_1 < \mathbf{f}_n, \mathbf{\Psi}_{1pq} >$$
$$+ t_2 < \mathbf{f}_n, \mathbf{\Psi}_{2pq} >)\mathbf{\Psi}_{1pq}$$
$$+ j\left[E_t^{(2)}\mathbf{\Psi}_2 + \frac{1}{\sqrt{A}}\sum_{n=1}^{N}\alpha_n\sum_{p=-\infty}^{\infty}\sum_{q=-\infty}^{\infty}(t_3 < \mathbf{f}_n, \mathbf{\Psi}_{1pq} >\right.$$
$$\left. + t_4 < \mathbf{f}_n, \mathbf{\Psi}_{2pq} >)\mathbf{\Psi}_{2pq}\right].$$
$$(28)$$

III. NUMERICAL RESULTS

Our study investigated the power reflection and transmission characteristics of meander-line polarizers with a chiral slab considering chirality effects. We plotted these coefficients as a function of frequency and of the incidence angle for a linearly polarized TM wave. The plotted values of these coefficients in all figures were normalized with respect to the incident power. We used the power conservation principle as a criterion to test the accuracy of the obtained results and thus prove the validity of our model. The sum of the co-TM-polarized and cross-TE-polarized power reflection and transmission coefficients amplitudes is equal to unity. The chirality admittance ξ indicates the degree of chirality, and its value is limited by $|\xi| \leq \sqrt{\varepsilon_c/\mu_c}$ [2].

We assumed that the meander-line is a two-dimensional infinite array of a perfectly conducting strip with a narrow width (with respect to λ). The geometrical dimensions chosen in the simulations (Fig. 1) were d_1=5 mm, d_2=10 mm (periodicities); $L_u=L_x$=2.5 mm (horizontal length); L_y=5 mm (vertical length); $t_y=t_x$=0.25 mm (thickness). During the calculations we tried different p and q values of the Floquet mode numbers and found that p=q=20 gave the best result, where the sum of the normalized power reflection and transmission coefficients were equal to unity [18]. For fixed values of p and q to give acceptable solutions, the number of segments n_1 (for lower horizontal branches), n_2 (for vertical branches), and n_3 (for upper horizontal branches) have to be correctly determined. The critical value of n_2 can be obtained from $n_2 = (2q+1)L_y/d_2$ [17]. In order for the segments to have the same length, the number of segments along the x-axis had to be $n_1=n_3=n_2/2$, since L_x and L_u are halves of L_y in this case.

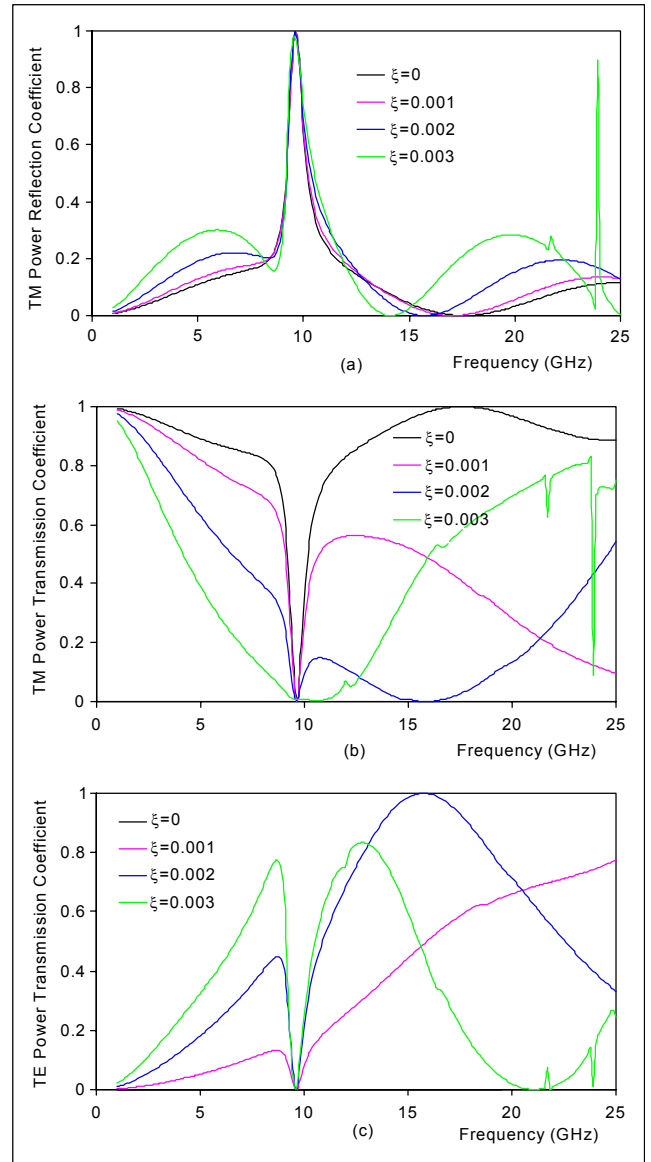Figures 2(a), 2(b), and 2(c) illustrate the co-polarized power

Fig. 2. Normalized power reflection and transmission coefficients against frequency for different values of chirality admittances; TM normal incidence, ε_r=2.0 and d=6.25 (λ/4) mm. (a) TM Power reflection coefficient, (b) TM Power transmission coefficient, (c) TE Power Transmission coefficient.

reflection and transmission coefficients and the cross-polarized power transmission coefficient, respectively. The cross-polarized power reflection coefficient was zero due to reciprocity and rotational symmetry. As Fig. 2(a) reveals, the co-polarized power reflection coefficient was unity around 10 GHz for four different values of chirality admittances. Thus, while the stop-band width is not a function of chirality, the transmission selectivity depicted in Fig. 2(b) is. Figure 2(c) shows that the cross-polarized power transmission coefficient approaches unity at a frequency band of around 15.5 GHz for

ξ=0.002. The polarization state of the transmitted wave is then converted from a TM mode to a TE mode at that frequency band.

Figures 3(a), 3(b), and 3(c) illustrate the co-polarized power reflection and the co-polarized power transmission coefficients and the cross-polarized power transmission coefficient as functions of the incidence angle, respectively. There is a Brewster angle only for ξ=0 and ξ=0.001 (Fig. 3(a)). The co-polarized power reflection coefficient shifts towards 90° with

a narrowing bandwidth and the Brewster angle disappears for ξ=0.003. The co-polarized power transmission coefficient is unity only at 72° for ξ=0. The magnitude of the cross-polarized power transmission coefficient is almost the same up to 70° (Fig. 3(c)).

IV. CONCLUSION

Chiral slabs can be used as a polarization transformer, which transforms any incoming polarization into any other polarization by rotating the axes of the two slabs of certain angles. A linearly polarized wave can be converted to a circularly polarized wave by using meander-line strips on a dielectric slab. In this study we examined the behavior of a chiral slab with a meander-line polarizer for different parameters. We presented power reflection and transmission coefficients as a function of frequency and of incidence angle for different values of the chirality admittance of the medium. Our results demonstrate that these coefficients can be changed effectively by using different chirality admittance values. The design parameters for a meander-line polarizer are the dimensions of the strips and the values of the dielectric slab. If dielectric slab is replaced by a chiral slab, the number of parameters will be increased by an effective parameter, namely, the chirality admittance. This presents an alternative for design parameters.

ACKNOWLEDGEMENTS

APPENDIX

The full expressions for the coefficients appearing in (14)-(17) are given below.

$$A_{L,Rpq}^{(m)}, B_{L,Rpq}^{(m)} = \left(\frac{Y_{L,Rpq}^{(m)}}{Y_c} \right)^{2-m} A_{L,Rpq} B_{L,Rpq},$$

$$Y_{L,Rpq}^{(1)} = Y_c \frac{k_{L,R}}{\gamma_{L,Rpq}}, \quad Y_{L,Rpq}^{(2)} = Y_c \frac{\gamma_{L,Rpq}}{k_{L,R}}, \quad Y_c = \sqrt{\frac{\varepsilon}{\mu}}$$

$$\begin{bmatrix} B_{Lpq} \\ B_{Rpq} \end{bmatrix} = \frac{1}{u} \begin{bmatrix} u_1 & u_2 \\ u_3 & u_4 \end{bmatrix} \begin{bmatrix} A_{Lpq} \\ A_{Rpq} \end{bmatrix}, \quad \begin{bmatrix} A_{Lpq} \\ A_{Rpq} \end{bmatrix} = \frac{1}{v} \begin{bmatrix} v_1 & v_2 \\ v_3 & v_4 \end{bmatrix} \begin{bmatrix} E_{rpq}^{(1)} \\ E_{rpq}^{(2)} \end{bmatrix}$$

$$\begin{bmatrix} E_{rpq}^{(1)} \\ E_{rpq}^{(2)} \end{bmatrix} = \frac{1}{r} \begin{bmatrix} r_1 & r_2 \\ r_3 & r_4 \end{bmatrix} \begin{bmatrix} E_{tpq}^{(1)} \\ E_{tpq}^{(2)} \end{bmatrix}$$

$$= \begin{bmatrix} t_1 & t_2 \\ t_3 & t_4 \end{bmatrix} \frac{1}{v} \begin{bmatrix} v_1 & v_2 \\ v_3 & v_4 \end{bmatrix} \frac{1}{r} \begin{bmatrix} r_1 & r_2 \\ r_3 & r_4 \end{bmatrix} \begin{bmatrix} I_{1pq} \\ I_{2pq} \end{bmatrix}$$
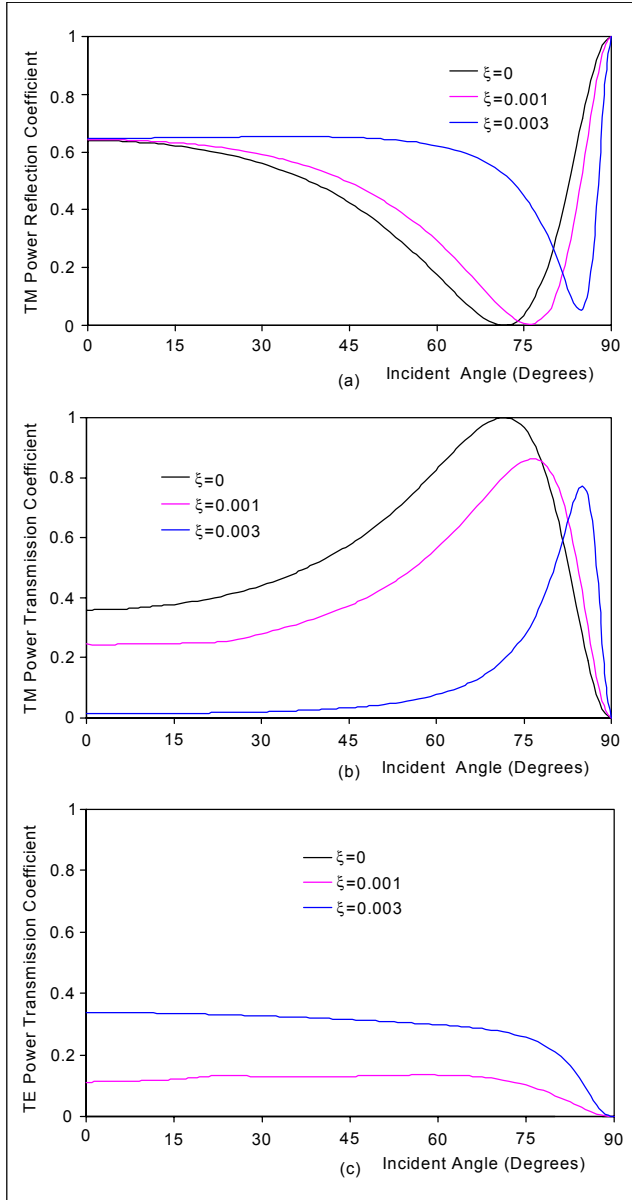

Fig. 3. Normalized power reflection and transmission coefficients against incident angle θ for different values of chirality admittances; TM incidence, ε_r=9 and d=6.25(λ/4) mm, f=12 GHz. (a) TM Power reflection coefficient, (b) TM Power Transmission coefficient, (c) TE Power Transmission coefficient.

$$u = (Y^{(1)} + Y_L^{(1)})(Y^{(2)} + Y_R^{(2)})Y_L^{(2)} + (Y^{(2)} + Y_L^{(2)})(Y^{(1)} + Y_R^{(1)})Y_R^{(2)}$$

$$u_1 = [(Y^{(1)} + Y_R^{(1)})(Y^{(2)} - Y_L^{(2)})Y_R^{(2)} \\ - (Y^{(2)} + Y_R^{(2)})(Y^{(1)} - Y_L^{(1)})Y_L^{(2)}]e^{-j2\gamma_L d}$$

$$u_2 = [(Y^{(1)} + Y_R^{(1)})(Y_R^{(2)} - Y^{(2)}) \\ - (Y^{(1)} - Y_R^{(1)})(Y^{(2)} + Y_R^{(2)})]Y_R^{(2)} e^{-j2(\gamma_L + \gamma_R)d}$$

$$u_3 = -[(Y^{(1)} - Y_L^{(1)})(Y_L^{(2)} + Y^{(2)}) \\ - (Y^{(1)} + Y_L^{(1)})(Y^{(2)} - Y_L^{(2)})]Y_L^{(2)} e^{-j2(\gamma_L + \gamma_R)d}$$

$$u_4 = -[(Y^{(1)} - Y_L^{(1)})(Y^{(2)} + Y_L^{(2)})Y_R^{(2)} \\ + (Y_R^{(2)} - Y^{(2)})(Y^{(1)} + Y_L^{(1)})Y_L^{(2)}]e^{-j2\gamma_R d}$$

$$v = (Y_L^{(2)} + Y_L^{(2)}u_1 + Y_R^{(2)}u_3)(-1 - u_2 + u_4) \\ - (1 - u_1 + u_3)(Y_R^{(2)} + Y_L^{(2)}u_2 + Y_R^{(2)}u_4)$$

$$v_1 = Y_c(-1 - u_2 + u_4),$$
$$v_2 = -Y_R^{(2)} - Y_L^{(2)}u_2 - Y_R^{(2)}u_4,$$
$$v_3 = Y_c(-1 + u_1 - u_3),$$
$$v_4 = Y_L^{(2)} + Y_L^{(2)}u_1 + Y_R^{(2)}u_3, r = r_1 r_4 - r_2 r_3$$

$$r_1 = v_2(-Y_L^{(2)} - Y_L^{(2)}u_1 + Y_R^{(2)}u_3) \\ + v_4(Y_R^{(2)} - Y_L^{(2)}u_2 + Y_R^{(2)}u_4) - Y^{(2)}$$

$$r_2 = j[Y_c v_2(-1 + u_1 + u_3) + Y_c v_4(-1 + u_2 + u_4)]$$

$$r_3 = -v_1(-Y_L^{(2)} - Y_L^{(2)}u_1 + Y_R^{(2)}u_3) - v_3(Y_R^{(2)} - Y_L^{(2)}u_2 + Y_R^{(2)}u_4)$$

$$r_4 = -j[Y_c v_1(-1 + u_1 + u_3) + Y_c v_3(-1 + u_2 + u_4) - Y^{(1)}]$$

$$t_1 = \frac{1}{Y_c}[Y_L^{(2)}e^{-j\gamma_L d} + \frac{1}{u}(Y_L^{(2)}u_1 e^{j\gamma_L d} + Y_R^{(2)}u_3 e^{j\gamma_R d})]$$

$$t_2 = \frac{1}{Y_c}[Y_R^{(2)}e^{-j\gamma_R d} + \frac{1}{u}(Y_L^{(2)}u_2 e^{j\gamma_L d} + Y_R^{(2)}u_4 e^{j\gamma_R d})],$$

$$t_3 = e^{-j\gamma_L d} - \frac{1}{u}(u_1 e^{j\gamma_L d} - u_3 e^{j\gamma_R d}),$$

$$t_4 = -e^{-j\gamma_R d} - \frac{1}{u}(u_2 e^{j\gamma_L d} - u_4 e^{j\gamma_R d})$$

$$\gamma_{L,Rpq} = \begin{cases} \sqrt{k_{L,R}^2 - |k_{Tpq}|^2}, & k_{L,R}^2 > |k_{Tpq}|^2 \\ -j\sqrt{|k_{Tpq}|^2 - k_{L,R}^2}, & k_{L,R}^2 < |k_{Tpq}|^2 \end{cases}$$

REFERENCES

[1] S. Bassiri, C.H. Papas, and N. Engheta, "Electromagnetic Wave Propagation Through a Dielectric-Chiral Interface and Through a Chiral Slab," *J. Opt. Soc. Am. A*, vol. 5, no. 9, Sept. 1988, pp. 1450-1459.

[2] N. Engheta and D.L. Jaggard, "Electromagnetic Chirality and Its Applications," *IEEE AP–S Newslett.*, vol. 30, no. 5, Oct. 1988, pp. 6-12.

[3] I.V. Lindell, A.H. Sihvola, S.A Tretyakov, and A.J. Viitanen, *Electromagnetic Waves in Chiral and Biisotropic Media*, Artech House, Norwood, NY, 1994.

[4] L. Young, L.A. Robinson, and C.A. Hacking, "Meander-Line Polarizer," *IEEE Trans. Propagat.*, vol. 21, no. 376, May 1973.

[5] R.S. Chu and K.M. Lee, "Analytical Model of a Multilayered Meander-Line Polarizer Plate with Normal and Oblique Plane Wave Incidence," *IEEE Trans. AP*, vol. 35, no. 6, June 1987, pp. 652-661.

[6] D.L. Jaggard, N. Engheta, M.W. Kowarz, P. Pelet, J.C. Liu, and Y. Kim, "Periodic Chiral Structures," *IEEE Trans. on Antennas and Propagat.*, vol. 37, no. 11, Nov. 1989, pp. 1447-1452.

[7] J. Lekner "Optical Properties of Isotropic Chiral Media," *Pure and Applied Optics: Journal of the European Optical Society Part A*, vol. 5, no. 4, July 1996, pp. 417-443.

[8] G. Plaza, F. Mesa, and M. Horno, "Study of the Dispersion Characteristics of Planar Chiral Lines," *IEEE Trans. Microwave Theory & Tech.*, vol. 46, 1998, pp. 1150-1157.

[9] A.J. Viitanen and P.P. Puska, "Reflection of Obliquely Incident Plane Wave from Chiral Slab Backed by Soft and Hard Surface," *IEE Proc.-Microw. Antennas Propag.*, vol. 146, no. 4, Aug. 1999, pp. 271-276.

[10] G. Scamarcio, F. Bilotti, A. Toscano, and L. Vegni, "Broad Band U-Slot Patch Antenna Loaded by Chiral Material," *Journal of Electromagnetic Waves and Applications*, vol. 15, no. 10, 2001, pp. 1303-1317.

[11] K.A. Vytovtov, "Analytical Investigation of Electromagnetic Waves in Bianisotropic Media," *IEE Proc.- Microw. Antennas Propag.*, vol. 148, no. 4, Aug. 2001, pp. 257-260.

[12] S. Uckun and T. Ege, "Computation of Susceptance for Thick Meander-Line Polarizer," *Electronic Lett.*, vol. 27, no. 22, Oct. 1991, pp. 2076-2077.

[13] N. Amitay, V. Galindo, and C.P. Wu, *Theory and Analysis of Phased Array Antennas*, Wiley-Intersection, New York, 1972.

[14] C.C. Chen, "Scattering by a Two-Dimensional Periodic Array of Conducting Plates," *IEEE Trans. AP*, vol. 18, no. 5, Sept. 1970, pp. 660-665.

[15] J.P. Montgomery, "Scattering by an Infinite Periodic Array of Thin Conductors on a Dielectric Sheet," *IEEE Trans. AP*, vol. 23, no. 1, Jan. 1975, pp. 70-75.

[16] R.F. Harrington, *Field Computation by Moment Methods*, MacMillan, New York, 1968.

[17] C. Terret, J.R. Levrel, and K. Mahdioubi, "Susceptance Computation of a Meander-Line Polarizer Layer," *IEEE Trans. on Antennas and Propagat.*, vol. AP-32, no. 9, Sept. 1984, pp. 1007-1011.

[18] K. Delihacioglu, *Power Reflection and Transmission Coefficient for a Chiral Slab and Meander-Line Polarizer with a Chiral Slab*, MS Thesis, University of Gaziantep, Nov. 1998.

Kemal Delihacıoğlu received the BS and MS degrees in electrical and electronic engineering from The University of Gaziantep, Turkey in 1995 and 1998. He is currently a PhD student and Research Assistant at the same university. His current research areas of interest include polarization, resonance, and scattering characteristics of chiral multilayer printed structures.

Savaş Uçkun received his BSc and MSc degrees in electrical engineering from the Middle East Technical University (METU), Gaziantep Engineering Faculty, Gaziantep, Turkey, in 1980 and 1983. He received a second MSc degree in computer science from the State University of New York at Albany in 1987 and his PhD degree in electrical engineering from METU in 1992. In 1980, he joined the Electrical Engineering Department of METU, Gaziantep, as a Research Assistant. Since 1999, he has been working as an Associate Professor in the Electrical and Electronic Engineering Department of the University of Gaziantep. In 1995 he was with the Department of Electrical Engineering of Syracuse University, NY, for three months as a Visiting Professor. His current research interests include propagation in a chiral medium and numerical solution of electromagnetic wave problems.